

Giant spontaneous Hall effect in a nonmagnetic Weyl-Kondo semimetal

S. Dzsaber¹, X. Yan¹, M. Taupin¹, G. Eguchi¹, A. Prokofiev¹, T. Shiroka^{2,3},
P. Blaha⁴, O. Rubel⁵, S. E. Grefe⁶, H.-H. Lai⁶, Q. Si⁶, and S. Paschen^{1,6,*}

¹Institute of Solid State Physics, Vienna University of Technology, 1040 Vienna, Austria

²Laboratorium für Festkörperphysik, ETH Zürich, 8093 Zurich, Switzerland

³Paul Scherrer Institut, 5232 Villigen PSI, Switzerland

⁴Institute of Materials Chemistry, Vienna University of Technology, 1040 Vienna, Austria

⁵Department of Materials Science and Engineering, McMaster University, 1280 Main Street
West, Hamilton, Ontario, Canada L8S 4L8

⁶Department of Physics and Astronomy, Rice Center for Quantum Materials, Rice University,
Houston, Texas 77005, USA

Exploring effects of topology in condensed matter systems¹ has led to the discovery of fundamentally new quantum phases and phenomena², including the spin Hall effect³, protected transport of helical fermions⁴, topological superconductivity⁵, and large nonlinear optical response^{6,7}. So far, focus has been on weakly interacting systems, but it is clear that the interplay of strong correlations and topology has many further surprises in store^{8,9}. Heavy fermion systems are a highly versatile platform to reveal them^{10,11}. Here we report the discovery of a giant spontaneous Hall effect in the noncentrosymmetric Kondo semimetal $\text{Ce}_3\text{Bi}_4\text{Pd}_3$ (ref 10), under preserved time reversal symmetry (TRS). We attribute it to Weyl nodes—singularities of the Berry curvature—Kondo-driven to the immediate vicinity of the Fermi level. We stress that this phenomenon is distinct from the previously detected anomalous Hall response in systems with broken TRS^{12–15} and that its characteristics require a description beyond the nonlinear quantum Hall effect¹⁶. The astonishingly large magnitude of the effect in even tiny electric and zero magnetic fields, as well as its robust bulk nature may aid the exploitation in topological quantum devices.

E-mail: *paschen@ifp.tuwien.ac.at

Weakly interacting Weyl semimetals have recently emerged as a new class of materials with topologically nontrivial bandstructure. Therein bulk 3D Dirac cones describing massless relativistic quasiparticles are stabilized by breaking either inversion symmetry (IS) or time reversal symmetry (TRS)¹⁷. Key experiments in their identification have been angle-resolved photoemission spectroscopy (ARPES)^{18–20} as well as magnetotransport measurements evidencing the chiral anomaly^{17,21,22}—charge pumping between a pair of Weyl nodes—in the form of a large negative longitudinal magnetoresistance. In a strongly correlated setting, however, both these techniques fail: ARPES experiments still lack the ultrahigh resolution needed to resolve strongly renormalized bands, and the largely reduced quasiparticle velocities of correlated materials make the observation of the chiral anomaly unlikely²². Thus, new tools have to be found to unveil the topological features of strongly correlated systems and pave the way for future discovery. Here we show that Hall effect measurements represent an ideal solution.

The material chosen for our study is the noncentrosymmetric heavy fermion semimetal $\text{Ce}_3\text{Bi}_4\text{Pd}_3$ (ref 10) that has recently been identified as a candidate Weyl-Kondo semimetal^{10,11}. Its low-temperature specific heat contains a giant electronic $c = \Gamma T^3$ term that was attributed to electronic states with extremely flat linear dispersion¹⁰, corresponding to a quasiparticle velocity v^* that is renormalized by a factor of 10^3 with respect to the Fermi velocity of a simple metal^{10,11}. This boosts the electronic ΓT^3 term to the point that it even overshoots the Debye βT^3 term of acoustic phonons¹⁰. To scrutinize this interpretation by other, more direct probes of topology is the motivation for the present work.

We start by showing that $\text{Ce}_3\text{Bi}_4\text{Pd}_3$ is governed by the Kondo interaction, and delineate the temperature and field range of Kondo coherence. The zero-field resistivity of $\text{Ce}_3\text{Bi}_4\text{Pd}_3$ increases weakly with decreasing temperature, whereas the nonmagnetic reference compound $\text{La}_3\text{Bi}_4\text{Pd}_3$ is metallic (Fig. 1a). This provides strong evidence that the semimetallic character of $\text{Ce}_3\text{Bi}_4\text{Pd}_3$ is due to the Kondo interaction. Below the single-ion Kondo temperature $T_K = 13$ K, identified by associating the material’s temperature-dependent entropy with a spin 1/2 ground state doublet of the Ce $4f^1$ wavefunction split by the Kondo interaction¹⁰, a broad shoulder in the resistivity at about 7 K signals the crossover to a Kondo coherent state (Fig. 1a). As shown in what follows, this is further supported by our magnetoresistance measurements (Fig. 1b, c).

Transverse magnetoresistance isotherms (Fig. 1b) in the incoherent regime between 7 and 30 K display the universal scaling typical of Kondo systems^{23,24}: $\rho_{xx}/\rho_{xx}(0\text{ T})$ vs B/B^* curves all collapse onto the theoretically predicted curve for an $S = 1/2$ Kondo impurity system²⁵, provided

a suitable scaling field B^* is chosen. The resulting B^* is linear in temperature (Fig. 1c). Fitting $B^* = B_0^*(1 + T/T^*)$ to the data (red straight line) yields $B_0^* = 10$ T and $T^* = 2.5$ K, which may be used as estimates of the field and temperature below which the system is fully Kondo coherent (blue area in Fig. 1d). Below 7 K, the scaling fails (Fig. 1b), as expected when crossing over from the incoherent to the Kondo coherent regime.

Before presenting our Hall effect results we show that, as anticipated, the chiral anomaly cannot be resolved in the Kondo coherent regime. We find that, at 2 K, the longitudinal and transverse magnetoresistance traces essentially collapse (Fig. 1e top). Because the amplitude c_a of the chiral anomaly, being inversely proportional to the density of states²², is expected to scale as $c_a \propto (v^*)^3$, it is severely suppressed by the strong correlations. The fact that, also at high temperatures, we do not observe signatures of the chiral anomaly (Fig. 1e bottom) demonstrates that no Weyl nodes are present in the uncorrelated bandstructure in the vicinity of the Fermi level, in agreement with our LDA bandstructure calculations (Fig. 4a).

Our key observation is a spontaneous Hall effect which appears in $\text{Ce}_3\text{Bi}_4\text{Pd}_3$ below T^* (Fig. 2a). The corresponding spontaneous Hall conductivity σ_{xy} reaches a considerable fraction of the corresponding quantum of 3D conductivity (Fig. 2b). The experiment, using a pseudo-AC mode (Methods), was not only carried out in zero external magnetic field, but also without any sample pre-magnetization process. Hall contact misalignment contributions were corrected for (Fig. S1) and, thus, can also not account for the effect. Moreover, being in the Kondo coherent regime, the local moments should be fully screened by the conduction electrons, resulting in a paramagnetic state. This is confirmed by state-of-the-art zero-field muon spin rotation (μSR) experiments. They reveal an extremely small electronic relaxation rate that is temperature-independent between 30 K and 250 mK (Fig. 2c; for two fully collapsing representative spectra, one well above and one well below T^* , see Fig. S7). This is unambiguous evidence that, in the investigated temperature range and in particular across T^* , TRS is preserved in $\text{Ce}_3\text{Bi}_4\text{Pd}_3$.

We also measured the Hall effect in finite applied magnetic fields. We observe that the field-dependent Hall resistivity isotherms, $\rho_{xy}(B)$, are fundamentally different below (Fig. 3a) and above T^* (Fig. 3b). Whereas above T^* , ρ_{xy} shows simple linear-in-field behavior consistent with a single hole-like band, strong nonlinearities appear below T^* . Most strikingly, a large even-in-field component $\rho_{xy}^{\text{even}} = [\rho_{xy}(B) + \rho_{xy}(-B)]/2$ is observed (Fig. 3c) that even overwhelms the usual odd-in-field component $\rho_{xy}^{\text{odd}} = [\rho_{xy}(B) - \rho_{xy}(-B)]/2$ (Fig. 3e). The nonlinear part of the latter, that scales with $[\rho_{xx} - \rho_{xx}(4\text{ K})]^2$ and is thus independent of the scattering time (Fig. 3f), is

theoretically expected¹² and experimentally observed¹⁵ in TRS broken Weyl semimetals, which is here realized by the finite magnetic field. The exciting new result, however, is the even-in- B component, which is the finite-field extension of the spontaneous Hall effect. Both are incompatible with the standard (magnetic field or magnetization induced) Hall conductivity mechanism, where the elements σ_{xy} of the fully antisymmetric Hall conductivity tensor may couple only to a physical quantity G that breaks TRS (i.e., $TG = -G$, where T is the time reversal operation)²⁶ and thus have to be an odd function of this quantity [e.g., $\sigma_{xy}(B) = -\sigma_{xy}(-B)$ where $G = B$].

The question then is how to understand the Hall response beyond this framework? Recent theoretical studies show that, in a current-carrying state of an IS breaking (but TRS preserving) material, a Hall conductivity can be generated by an anomalous velocity associated with the Berry curvature in momentum space¹⁶

$$\sigma_{xy} = \frac{e^2}{\hbar} \int \frac{d^3k}{(2\pi)^3} f(\mathbf{k}) \Omega_z^{\text{odd}}(\mathbf{k}), \quad (1)$$

where $f(\mathbf{k})$ is the nonequilibrium electron distribution function in an applied electric field \mathcal{E}_x and Ω_z^{odd} the Berry curvature, which is odd in \mathbf{k} [$\Omega^{\text{odd}}(\mathbf{k}) = -\Omega^{\text{odd}}(-\mathbf{k})$] for systems with broken IS (ref 27). Such a state breaks TRS at the thermodynamic level, as $f(\mathbf{k})$ can be maintained only at the cost of entropy production ($\dot{S} = j_x \mathcal{E}_x$, where j_x is the current density). It is this macroscopically broken TRS that allows for a finite Hall voltage. We see that $T\Omega^{\text{odd}} = -\Omega^{\text{odd}}$ and thus $\sigma_{xy}(\Omega^{\text{odd}}) = -\sigma_{xy}(-\Omega^{\text{odd}})$. In this case, $\sigma_{xy}(B)$ does not need to be odd in B and a finite σ_{xy} does not even require the presence of any B at all. In fact, the only role the magnetic field plays in this topological Hall effect is to reduce its magnitude as it pushes the material away from full Kondo coherence, analogous to what happens when heating the material beyond T^* (Fig. 3c). The observations of a spontaneous Hall effect (Fig. 2) and an even-in-field Hall conductivity (Fig. 3) in $\text{Ce}_3\text{Bi}_4\text{Pd}_3$ are smoking-gun evidences that the physical quantity underlying the phenomenon is not a magnetic order parameter (coupled linearly to B), as otherwise σ_{xy} would necessarily be completely odd in B . That the spontaneous Hall current is indeed carried by $f(\mathbf{k})$ is further supported by the linear relationship between σ_{xy} and σ_{xx} in the Kondo coherent regime (Fig. 2b), consistent with a linear dependence on scattering time ($\sigma_{xy} \sim \tau$) and thus the nonequilibrium nature of the effect.

Because according to Eqn. 1 the topological Hall current is carried by $f(\mathbf{k})$, σ_{xy} will depend on \mathcal{E}_x , and thus the Hall response $j_y = \sigma_{xy}(\mathcal{E}_x) \cdot \mathcal{E}_x$ is expected to be nonlinear in \mathcal{E}_x . By Taylor expanding $f(\mathbf{k})$ around the equilibrium (Fermi-Dirac) distribution function $f_0(\mathbf{k})$, a second

harmonic response was derived¹⁶, which we have set out to probe by investigating both the dependence of the Hall response on the electric field (or current) strength and by analysing the different components of the Hall response under AC current drive. The former experiments reveal that the spontaneous Hall voltage V_{xy}^{DC} under DC current drive is indeed nonlinear in the applied electric current I^{DC} (Fig. S4a right). It can be decomposed into a linear- and a quadratic-in- I^{DC} contribution. This is in contrast to the longitudinal voltage V_{xx}^{DC} that is linear in current, representing an Ohmic electrical resistivity (Fig. S4a left). In our AC experiments, in response to an excitation at frequency ω we detect voltage contributions at 1ω , 2ω , and 0ω . Whereas $V_{xy}^{1\omega}$ is linear in $I^{1\omega}$ (Fig. S5b), both $V_{xy}^{2\omega}$ and $V_{xy}^{0\omega}$ are quadratic in $I^{1\omega}$ (Fig. 2d,e). These three responses as well as the DC response described above appear simultaneously, as Kondo coherence develops with decreasing temperature (Fig. 2f), and must thus have a common origin.

The nonlinear spontaneous Hall voltage terms ($V_{xy}^{2\omega}$, $V_{xy}^{0\omega}$, $V_{xy}^{\text{DC}} \sim I^2$) are expected within the perturbative treatment¹⁶ of the topological (or quantum nonlinear) Hall effect of Eqn. 1. In what follows we compare the magnitude of these terms found in our experiments with *ab initio* calculations for several weakly interacting Weyl semimetals²⁸. Within the perturbative approach^{16,28}, the Berry curvature dipole

$$D_{xz} = \int \frac{d^3k}{(2\pi)^3} f_0(\mathbf{k}) \frac{\partial \Omega_z^{\text{odd}}}{\partial k_x} \quad (2)$$

as well as $\sigma_{xy} = e^3 \tau D_{xz} / (2\hbar^2) \cdot \mathcal{E}_x$ can be computed from the electronic band structure as function of the chemical potential. $\tan(\Theta) \equiv \sigma_{xy} / \sigma_{xx}$, where σ_{xx} is the normal (1ω) longitudinal conductivity, was found to be at maximum of the order 10^{-4} for a scattering time $\tau = 10$ ps and an electric field of $\mathcal{E}_x = 10^2$ V/m, corresponding to $\tan(\Theta) / \mathcal{E}_x \leq 10^{-6}$ m/V (ref 28). For $\text{Ce}_3\text{Bi}_4\text{Pd}_3$, we have measured values as large as 3×10^{-3} m/V for this ratio in the second harmonic channel (Fig. 2d). Indeed, an effect that is at least three orders of magnitude smaller would be difficult to resolve experimentally, explaining why for weakly interacting nonmagnetic Weyl semimetals it has not been reported. The giant value we observe is even more surprising as it is obtained in a bulk semimetal, without any chemical potential tuning. Experimentally, such tuning is limited to the case of (quasi) 2D insulators/semiconductors, and has indeed recently revealed a 2ω Hall voltage in bilayer²⁹ and multilayer³⁰ WTe_2 ; we estimate the maximum values reached there to be $\tan(\Theta) \approx 5 \times 10^{-3}$ and 10^{-4} , and $\tan(\Theta) / \mathcal{E}_x \approx 3 \times 10^{-6}$ m/V and 10^{-8} m/V, respectively. As these materials are gapped, there is no Berry curvature divergence, explaining the comparably small magnitude of the effect.

The linear-in-current DC as well as the (first harmonic) 1ω AC contribution to V_{xy} , by contrast, are unexpected in the perturbative treatment¹⁶. Intriguingly, these contributions, with $\tan(\Theta)$ in the range of 0.15 to 0.5 (Fig. 2b and Fig. S6b), are even much larger than the 2ω effect quantified above. In what follows we show that the striking deviations from simple expectations^{16,28}, most notably the giant enhancement of the spontaneous nonlinear Hall effect, the even-in-field Hall conductivity, and the appearance of a linear-in-field (first harmonic) contribution—arizes naturally in a Weyl-Kondo semimetal.

Here, the Weyl nodes, where the Berry curvature is singular, are essentially pinned to the Fermi level^{10,11} and the application of even small electric fields has a nonperturbative effect (see Supplementary Information for an expanded discussion). A simple Taylor expansion of $f(\mathbf{k})$ around $f_0(\mathbf{k})$, as done in ref 16, will therefore fail to describe the situation. Quantitative predictions from fully nonequilibrium transport calculations based on an *ab initio* electronic bandstructure in the limit of strong Coulomb interaction and strong spin-orbit coupling are elusive to date. Thus, instead, we here present a conceptual understanding. While (generically tilted) Weyl cones are present already in the noninteracting bandstructure of $\text{Ce}_3\text{Bi}_4\text{Pd}_3$ (Fig. 4a and Supplementary Information), it is the Kondo interaction that pushes them to the immediate vicinity of the Fermi level (Fig. 4b), as indicated by calculations for a periodic Anderson model with tilted Weyl cones in the bare conduction electron band (see ref 11 and Supplementary Information) and evidenced by thermodynamic measurements¹⁰. In the resulting tilted Weyl-Kondo semimetal, each Weyl node will thus be asymmetrically surrounded by a tiny Fermi pocket, with the smallest distance between node and Fermi surface denoted by k_W (Fig. 4c). The application of even small electric fields will then induce shifts $\Delta\mathbf{k}$ in the distribution function $f(\mathbf{k})$ that are sizeable compared to k_W , and possibly even compared to the Fermi wavevector k_F , thus driving the system to a fully nonequilibrium regime (Fig. 4d). In this setting, a nonperturbative approach is needed, and will allow for the appearance of terms beyond the second harmonic one predicted by Sodemann and Fu¹⁶, most notably the experimentally observed first harmonic one (Supplementary Information). As the applied \mathcal{E} field can then no longer be considered as a probing field, it introduces a directionality on top of the crystal's space group symmetry and the selection rules, that hold in the perturbative regime, will be violated.

In conclusion, our Hall effect measurements have unambiguously identified a giant Berry curvature contribution in a time-reversal invariant material, the noncentrosymmetric heavy fermion semimetal $\text{Ce}_3\text{Bi}_4\text{Pd}_3$. The Hall angle per applied electric field, a figure-of-merit of the effect,

is enhanced by orders of magnitude over values expected for weakly interacting systems, which we attribute to Kondo-driven tilted Weyl nodes very close to the Fermi surface. The experiments established here should allow for a ready identification of other strongly correlated nonmagnetic Weyl semimetals, be it in heavy fermion compounds or in other materials classes, thereby enabling much needed systematic studies of the interplay of strong correlations and topology. Finally, the discovered effect being present in a 3D material, in the absence of any magnetic fields and under only tiny driving electric fields, holds great promise for the development of robust topological quantum devices.

-
1. Haldane, F. Nobel Lecture: Topological quantum matter. *Rev. Mod. Phys.* **89**, 040502 (2017).
 2. Focus Issue “Topological matter”. *Nat. Phys.* **12**, 615 (2016).
 3. König, M., Wiedmann, S., Brüne, C., Roth, A., Buhmann, H., Molenkamp, L. W., Qi, X. & Zhang, S. Quantum spin Hall insulator state in HgTe quantum wells. *Science* **318**, 766 (2007).
 4. Hsieh, D., Xia, Y., Qian, D., Wray, L., Dil, J. H., Meier, F., Osterwalder, J., Patthey, L., Checkelsky, J. G., Ong, N. P., Fedorov, A. V., Lin, H., Bansil, A., Grauer, D., Hor, Y. S., Cava, R. J. & Hasan, M. Z. A tunable topological insulator in the spin helical Dirac transport regime. *Nature* **460**, 1101 (2009).
 5. Sasaki, S., Kriener, M., Segawa, K., Yada, K., Tanaka, Y., Sato, M. & Ando, Y. Topological superconductivity in $\text{Cu}_x\text{Bi}_2\text{Se}_3$. *Phys. Rev. Lett.* **107**, 217001 (2011).
 6. Wu, L., Patankar, S., Morimoto, T., Nair, N. L., Thewalt, E., Little, A., Analytis, J. G., Moore, J. E. & Orenstein, J. Giant anisotropic nonlinear optical response in transition metal mononictide Weyl semimetals. *Nat. Phys.* **13**, 350 (2016).
 7. Ma, Q., Xu, S.-Y., Chan, C.-K., Zhang, C.-L., Chang, G., Lin, Y., Xie, W., Palacios, T., Lin, H., Jia, S., Lee, P. A., Jarillo-Herrero, P. & Gedik, N. Direct optical detection of Weyl fermion chirality in a topological semimetal. *Nat. Phys.* **13**, 842 (2017).
 8. Yang, B.-J., Moon, E.-G., Isobe, H. & Nagaosa, N. Quantum criticality of topological phase transitions in three-dimensional interacting electronic systems. *Nat. Phys.* **10**, 774 (2014).
 9. Castelvechi, D. The shape of things to come. *Nature* **547**, 272 (2017).
 10. Dzsaber, S., Prochaska, L., Sidorenko, A., Eguchi, G., Svagera, R., Waas, M., Prokofiev, A., Si, Q. & Paschen, S. Kondo insulator to semimetal transformation tuned by spin-orbit coupling. *Phys. Rev. Lett.* **118**, 246601 (2017).
 11. Lai, H.-H., Greife, S. E., Paschen, S. & Si, Q. Weyl-Kondo semimetal in heavy-fermion systems. *Proc. Natl. Acad. Sci. U.S.A.* **115**, 93 (2018).
 12. Nagaosa, N., Sinova, J., Onoda, S., MacDonald, A. H. & Ong, N. P. Anomalous Hall effect. *Rev. Mod. Phys.* **82**, 1539 (2010).
 13. Machida, Y., Nakatsuji, S., Onoda, S., Tayama, T. & Sakakibara, T. Time-reversal symmetry breaking and spontaneous Hall effect without magnetic dipole order. *Nature* **463**, 210 (2010).
 14. Nakatsuji, S., Kiyohara, N. & Higo, T. Large anomalous Hall effect in a non-collinear antiferromagnet at room temperature. *Nature* **527**, 212 (2015).

15. Liu, E., Sun, Y., Kumar, N., Muechler, L., Sun, A., Jiao, L., Yang, S.-Y., Liu, D., Liang, A., Xu, Q., Kroder, J., Süß, V., Borrmann, H., Shekhar, C., Wang, Z., Xi, C., Wang, W., Schnelle, W., Wirth, S., Chen, Y., Goennenwein, S. T. B. & Felser, C. Giant anomalous Hall effect in a ferromagnetic kagome-lattice semimetal. *Nat. Phys.* **14**, 1125 (2018).
16. Sodemann, I. & Fu, L. Quantum nonlinear Hall effect induced by Berry curvature dipole in time-reversal invariant materials. *Phys. Rev. Lett.* **115**, 216806 (2015).
17. Armitage, N. P., Mele, E. J. & Vishwanath, A. Weyl and Dirac semimetals in three-dimensional solids. *Rev. Mod. Phys.* **90**, 015001 (2018).
18. Huang, S.-M., Xu, S.-Y., Belopolski, I., Lee, C.-C., Chang, G., Wang, B., Alidoust, N., Bian, G., Neupane, M., Zhang, C., Jia, S., Bansil, A., Lin, H. & Hasan, M. Z. A Weyl fermion semimetal with surface Fermi arcs in the transition metal monpnictide TaAs class. *Nat. Commun.* **6**, 7373 (2015).
19. Xu, S.-Y., Belopolski, I., Alidoust, N., Neupane, M., Bian, G., Zhang, C., Sankar, R., Chang, G., Yuan, Z., Lee, C.-C., Huang, S.-M., Zheng, H., Ma, J., Sanchez, D. S., Wang, B., Bansil, A., Chou, F., Shibaev, P. P., Lin, H., Jia, S. & Hasan, M. Z. Discovery of a Weyl fermion semimetal and topological Fermi arcs. *Science* **349**, 613 (2015).
20. Xu, N., Weng, H. M., Lv, B. Q., Matt, C. E., Park, J., Bisti, F., Strocov, V. N., Gawryluk, D., Pomjakushina, E., Conder, K., Plumb, N. C., Radovic, M., Auts, G., Yazyev, O. V., Fang, Z., Dai, X., Qian, T., Mesot, J., Ding, H. & Shi, M. Observation of Weyl nodes and Fermi arcs in tantalum phosphide. *Nat. Commun.* **7**, 11006 (2016).
21. Huang, X., Zhao, L., Long, Y., Wang, P., Chen, D., Yang, Z., Liang, H., Xue, M., Weng, H., Fang, Z., Dai, X. & Chen, G. Observation of the chiral-anomaly-induced negative magnetoresistance in 3D Weyl semimetal TaAs. *Phys. Rev. X* **5**, 031023 (2015).
22. Zhang, C.-L., Xu, S.-Y., Belopolski, I., Yuan, Z., Lin, Z., Tong, B., Bian, G., Alidoust, N., Lee, C.-C., Huang, S.-M., Chang, T.-R., Chang, G., Hsu, C.-H., Jeng, H.-T., Neupane, M., Sanchez, D. S., Zheng, H., Wang, J., Lin, H., Zhang, C., Lu, H.-Z., Shen, S.-Q., Neupert, T., Zahid Hasan, M. & Jia, S. Signatures of the Adler–Bell–Jackiw chiral anomaly in a Weyl fermion semimetal. *Nat. Commun.* **7**, 10735 (2016).
23. Singh, Y. P., Haney, D. J., Huang, X. Y., Lum, I. K., White, B. D., Dzero, M., Maple, M. B. & Almasan, C. C. From local moment to mixed-valence regime in $\text{Ce}_{1-x}\text{Yb}_x\text{CoIn}_5$ alloys. *Phys. Rev. B* **89**, 115106 (2014).
24. Maple, M. B., Butch, N. P., Frederick, N. A., Ho, P.-C., Jeffries, J. R., Sayles, T. A., Yanagisawa, T.,

- Yuhasz, W. M., Chi, S., Kang, H. J., Lynn, J. W., Dai, P., McCall, S. K., McElfresh, M. W., Fluss, M. J., Henkie, Z. & Pietraszko, A. Field-dependent ordered phases and Kondo phenomena in the filled skutterudite compound $\text{PrOs}_4\text{As}_{12}$. *Proc. Natl. Acad. Sci. U.S.A.* **103**, 6783 (2006).
25. Schlottmann, P. Bethe-Ansatz solution of the ground-state of the SU $(2j + 1)$ Kondo (Coqblin-Schrieffer) model: Magnetization, magnetoresistance and universality. *Z. Phys. B* **51**, 223 (1983).
26. Casimir, H. B. G. On Onsager's principle of microscopic reversibility. *Rev. Mod. Phys.* **17**, 343 (1945).
27. Xiao, D., Chang, M.-C. & Niu, Q. Berry phase effects on electronic properties. *Rev. Mod. Phys.* **82**, 1959 (2010).
28. Zhang, Y., Sun, Y. & Yan, B. Berry curvature dipole in Weyl semimetal materials: An *ab initio* study. *Phys. Rev. B* **97**, 041101 (2018).
29. Ma, Q., Xu, S.-Y., Shen, H., MacNeill, D., Fatemi, V., Chang, T.-R., Mier Valdivia, A. M., Wu, S., Du, Z., Hsu, C.-H., Fang, S., Gibson, Q. D., Watanabe, K., Taniguchi, T., Cava, R. J., Kaxiras, E., Lu, H.-Z., Lin, H., Fu, L., Gedik, N. & Jarillo-Herrero, P. Observation of the nonlinear Hall effect under time-reversal-symmetric conditions. *Nature* **565**, 337 (2019).
30. Kang, K., Li, T., Sohn, E., Shan, J. & Mak, K. F. Nonlinear anomalous Hall effect in few-layer WTe_2 . *Nat. Mater.* **18**, 324 (2019).

Acknowledgements

The authors thank J.-C. Orain for technical assistance during the μSR experiments and J. Mesot and D. A. Zocco for fruitful discussion. The team in Vienna acknowledges financial support from the Austrian Science Fund (FWF grant No. P29296-N27 and DK W1243). T.S. acknowledges support from the Swiss National Science Foundation (SNF Grant No. 200021-169455). Work at Rice was in part supported by the NSF (DMR-1920740) and the Robert A. Welch Foundation (C-1411), and by a Ulam Scholarship from the Center for Nonlinear Studies at Los Alamos National Laboratory.

Author Contributions

S.P. initiated and lead the study. S.D., X.Y., and A.P. synthesized and characterized the material. S.D. and M.T. performed and analyzed the magnetotransport measurements. G.E. contributed to the data analysis. T.S. and S.D. performed the μSR investigation. P.B. and O.R. performed the *ab initio* study, S.E.G., H.H.L., and Q.S. the study of the Weyl-Kondo model. S.D. and S.P. prepared the manuscript, with input from all authors. All authors contributed to the discussion.

Author Information

Reprints and permissions information is available at www.nature.com/reprints. The authors declare no competing financial interests. Readers are welcome to comment on the online version of the paper. Correspondence and requests for materials should be addressed to S.P. (paschen@ifp.tuwien.ac.at).

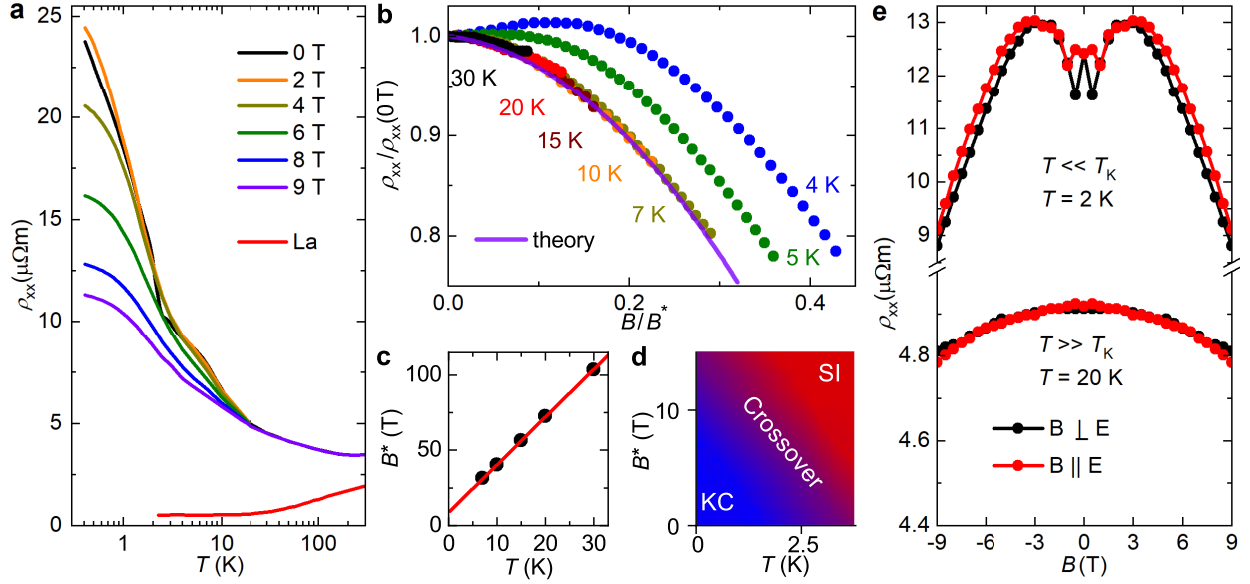


FIG. 1: Electrical resistivity and magnetoresistance of $\text{Ce}_3\text{Bi}_4\text{Pd}_3$. **a**, Temperature-dependent electrical resistivity ρ_{xx} of $\text{Ce}_3\text{Bi}_4\text{Pd}_3$ in various magnetic fields applied perpendicular to the electric field ($B \perp E$, transverse magnetoresistance) and of the nonmagnetic reference compound $\text{La}_3\text{Bi}_4\text{Pd}_3$ in zero field (red). **b**, Transverse magnetoresistance scaled to its zero-field value vs scaled magnetic field B/B^* , showing the collapses of data above 7 K onto the universal curve²⁵ (violet) expected for an $S = 1/2$ Kondo impurity system in the incoherent regime, and a breakdown of the scaling for temperatures below 7 K (shown here by using B^* from the linear fit in **c**,—also other choices of B^* cannot achieve scaling). **c**, Scaling field B^* , as determined in **b**, vs temperature, showing a linear-in- T behavior as expected for a Kondo system in the single-impurity regime. Fitting $B^* = B_0^*(1 + T/T^*)$ to the data (red straight line) yields $B_0^* = 10$ T and $T^* = 2.5$ K. **d**, Temperature-field phase diagram displaying the single impurity (SI) and Kondo coherent (KC) regime as derived in **c**. **e**, Transverse (black) and longitudinal (red, $B||E$) magnetoresistance for temperatures well below (top) and well above T_K (bottom). The data were symmetrized to remove any spurious Hall resistivity contribution, and mirrored on the vertical axis for clarity.

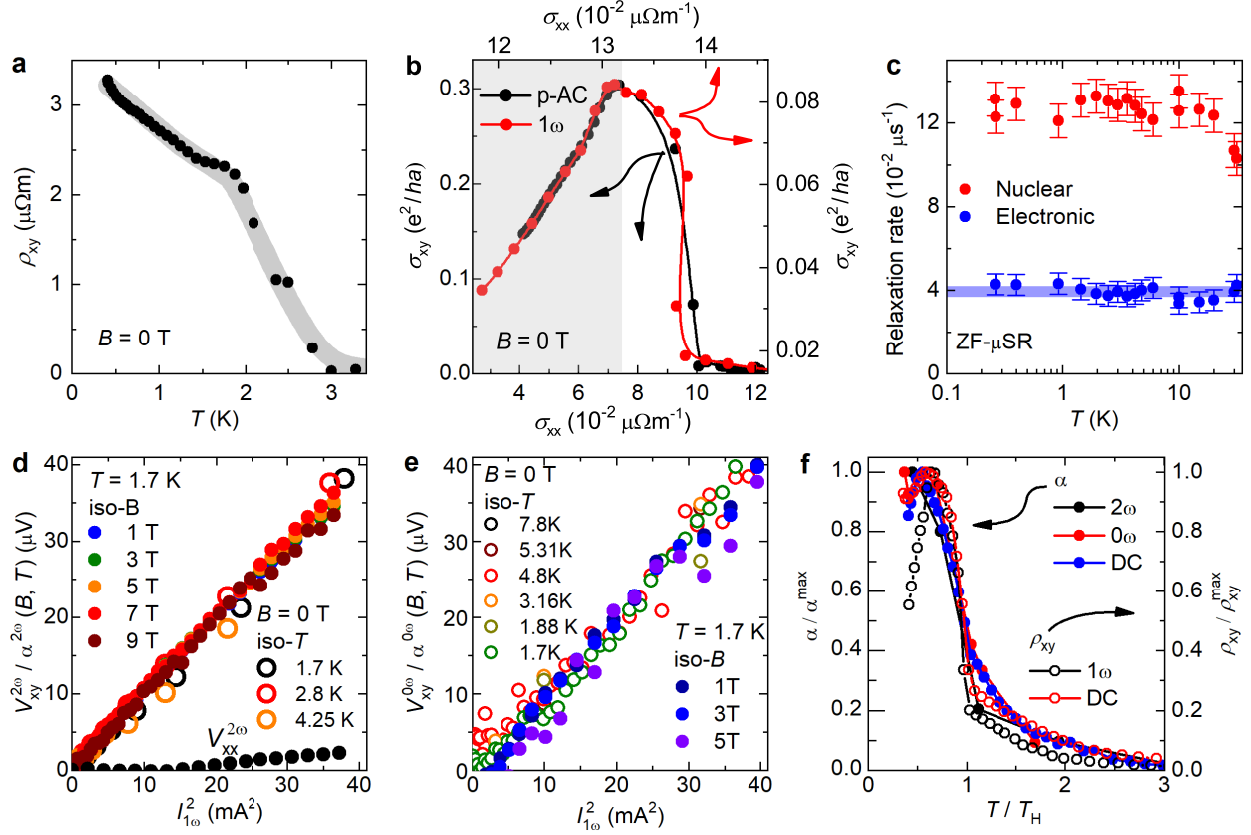


FIG. 2: Spontaneous Hall effect of $\text{Ce}_3\text{Bi}_4\text{Pd}_3$. **a**, Temperature-dependent DC Hall resistivity ρ_{xy} in zero external magnetic field, showing a pronounced spontaneous Hall effect below 3 K.

Data were taken without prior application of magnetic fields. **b**, Spontaneous DC Hall conductivity σ_{xy} in units of the 3D conductivity quantum vs longitudinal conductivity σ_{xx} , with temperature as implicit parameter, for the DC response of the sample in **a** (bottom and left axes, black), and for the 1ω response in an AC experiment on a sample from a different batch (top and right axes, red), both in zero magnetic field. In the Kondo coherent regime (grey shading), σ_{xy} is linear in σ_{xx} . **c**, Temperature-dependent nuclear and electronic contributions to the muon spin relaxation rate obtained from ZF- μ SR measurements. The electronic contribution is extremely small and temperature-independent within the error bars. **d**, Scaled 2ω spontaneous Hall voltage vs square of 1ω driving electrical current in zero magnetic field for different temperatures, and at 1.7 K for various magnetic fields. **e**, Quantities analogous to **d** for the 0ω spontaneous Hall voltage. **f**, Scaled coefficients of square-in-current response $\alpha^{2\omega,0\omega,\text{DC}}$ from panel **d**, **e**, and Fig. S4, respectively (left axis), and linear-in-current response $\rho_{xy}^{1\omega,\text{DC}}$ from panel **b** (right axis), as function of scaled temperature (T_H is the onset temperature for a large spontaneous Hall signal).

The absolute values of $\alpha^{\text{max},i}$, $\rho_{xy}^{\text{max},i}$, and T_H are listed in Table S1.

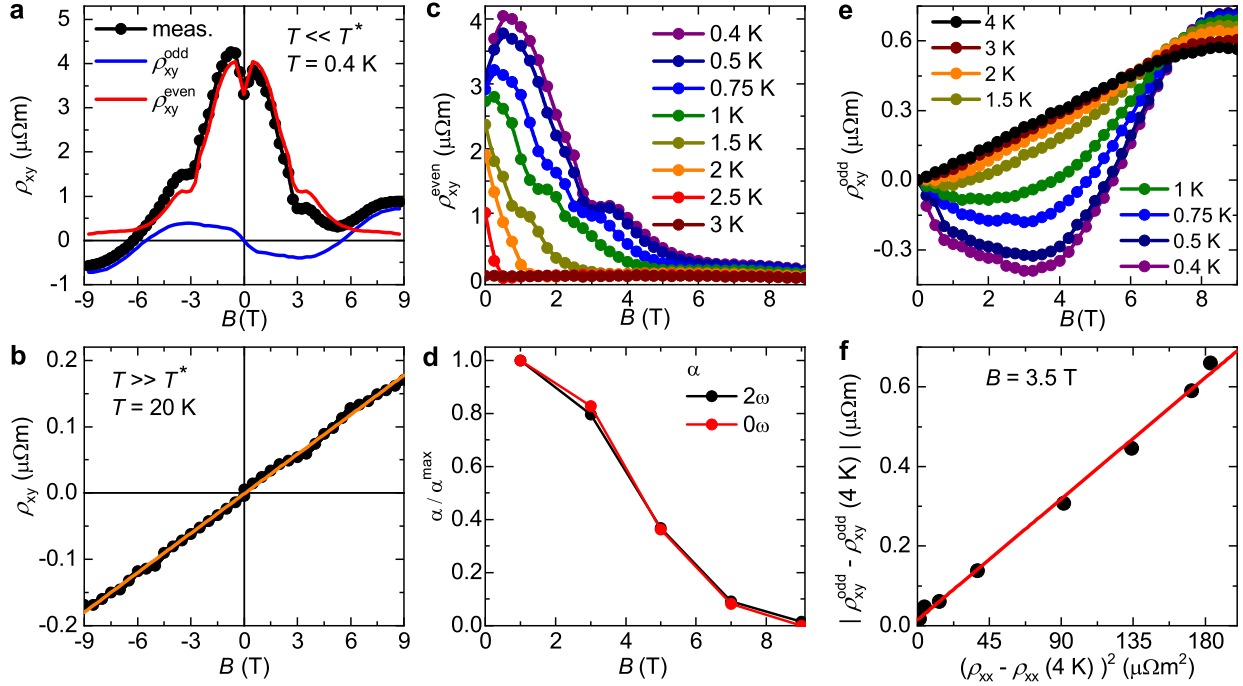


FIG. 3: Hall resistivity of $\text{Ce}_3\text{Bi}_4\text{Pd}_3$ in external magnetic fields. **a**, In the Kondo coherent regime below T^* and B_0^* (Fig. 1d), the magnetic field-dependent DC Hall resistivity $\rho_{xy}(B)$ shows a pronounced anomalous Hall effect (AHE) and can be decomposed into an odd-in- B $\rho_{xy}^{\text{odd}}(B)$ (blue) and an even-in- B $\rho_{xy}^{\text{even}}(B)$ (red) component. **b**, Above T^* , $\rho_{xy}(B)$ is dominated by a linear-in- B normal Hall effect. **c**, $\rho_{xy}^{\text{even}}(B, T)$ is suppressed for $T > T^*$ and $B > B_0^*$. **d**, Scaled coefficients of the 2ω and 0ω Hall voltage in an AC experiment (from Fig. 2d,e) as function of magnetic field. **e**, Below T^* and B_0^* , $\rho_{xy}^{\text{odd}}(B, T)$ shows a pronounced AHE on top of a linear background from the normal Hall effect. **f**, Amplitude of the odd-in- B AHE, estimated as the total odd-in- B component at 3.5 T (location of extremum) minus its value at 4 K, where the effect has disappeared (see **e**), vs the square of the corresponding magnetoresistance difference $[\rho_{xx}(T) - \rho_{xx}(4\text{ K})]$ at 3.5 T, with T as implicit parameter. The observed quadratic dependence (red straight line) is in remarkable agreement with expectations for the AHE due to broken TRS as B is applied.

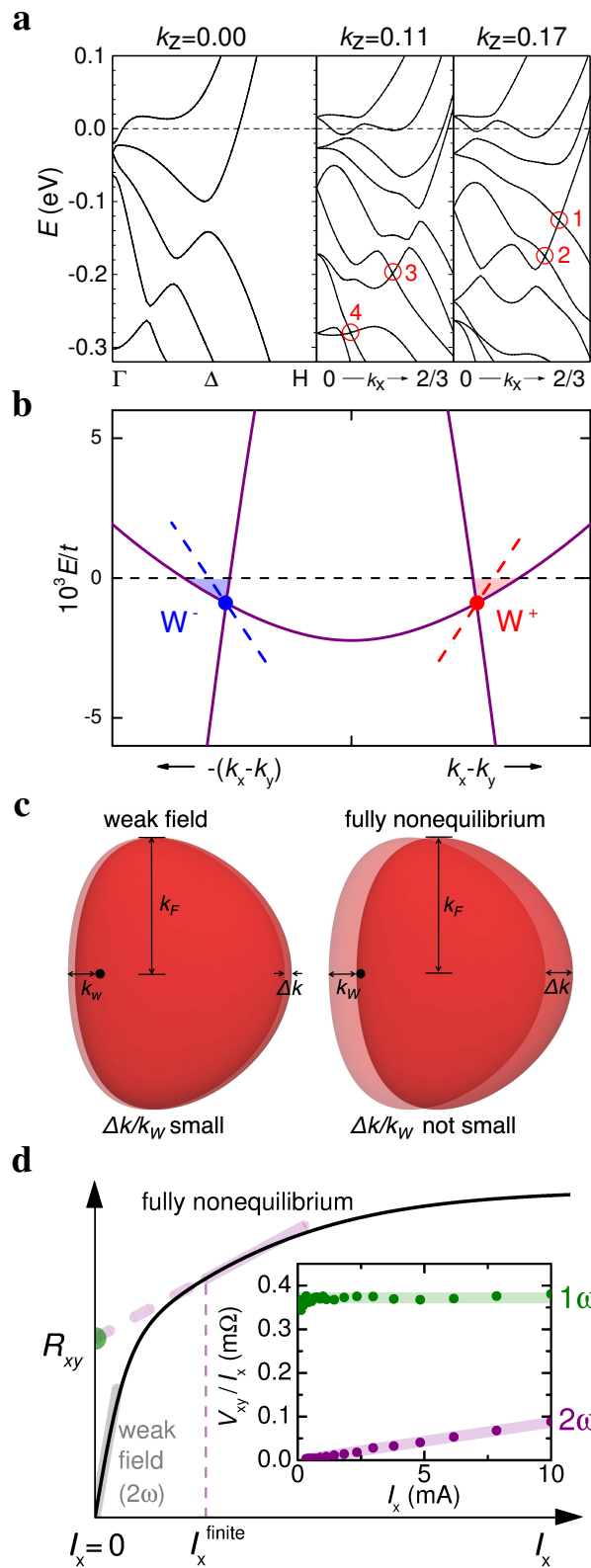


FIG. 4: **Theoretical description of Weyl-Kondo physics in $\text{Ce}_3\text{Bi}_4\text{Pd}_3$.** **a**, *Ab initio* band structure of $\text{Ce}_3\text{Bi}_4\text{Pd}_3$, with $4f$ electrons in the core. In the k_x - k_z plane, four different Weyl nodes (1-4) are identified. 1 and 4 are most strongly tilted (Supplementary Information). **b** Dispersion across a pair of Weyl (W^+) and anti-Weyl (W^-) nodes for a Weyl-Kondo model with tilted Weyl cones (Supplementary Information). Energy is expressed in units of the conduction electron bandwidth t . The Kondo interaction pushes the Weyl nodes, that are present in the bare conduction electron band far away from the Fermi energy, to the immediate vicinity of the Fermi

cont. FIG. 4: ... level (here at $E/t = 0$, slightly above the Weyl nodes). **c**, Sketch of a Fermi pocket around the Weyl node W^+ in **b** (dot) in zero electric field (light red) and its nonequilibrium counterpart with driving electric field (red), in the weak-field regime (left) and the fully nonequilibrium regime (right). **d**, Sketch of the driving current-induced Hall resistance $R_{xy} = V_{xy}/I_x$, displaying the weak-field and fully nonequilibrium regimes. **inset**, Experimental results for $\text{Ce}_3\text{Bi}_4\text{Pd}_3$, demonstrating the simultaneous presence of a spontaneous Hall signal in both the 2ω ($V_{xy} \sim I_x^2$) and 1ω ($V_{xy} \sim I_x$) channel. The sum of both contributions corresponds to a linear-in- I_x Hall resistance with a finite offset (violet line with green dot in main panel), which is a characteristic of the fully nonequilibrium regime.

Methods

A. Synthesis

Single crystals of $\text{Ce}_3\text{Bi}_4\text{Pd}_3$ and the nonmagnetic reference compound $\text{La}_3\text{Bi}_4\text{Pd}_3$ were synthesized using a Bi-flux method¹⁰. Their stoichiometry, phase purity, and crystal structure were verified using powder X-ray diffraction, scanning electron microscopy, energy dispersive X-ray spectroscopy, and Laue diffraction.

B. Measurement setups

Magnetotransport measurements were performed using various devices: two Quantum Design Physical Property Measurement Systems, in part with ^3He or vertical rotator option, and an Oxford ^4He flow cryostat using a Stanford Research SR830 lock-in amplifier. In the former, we used a pseudo-AC technique (p-AC), in the latter a standard AC technique with lock-in detection. Electrical contacts for these measurements were made by spot welding 12 μm diameter gold wires to the samples in a 5- or 6-wire configuration, depending on the crystal size. Oriented single crystals were studied with the driving electrical current along different crystallographic directions (approximately along $[103]$, $[111]$, and $[100]$).

The μSR measurements were performed at the Dolly spectrometer of the Swiss Muon Source at Paul Scherrer Institut, Villigen. The single crystals were arranged to form a mosaic with about 1 cm diameter and a thickness of about 0.5 mm, glued on top of a thin copper foil solidly clamped to a copper sample holder, thus optimally using the muon beam cross section, minimizing the background from the sample holder, and guaranteeing good thermal contact. Combined with active vetoing, this setup resulted in very low spurious background signals. A cold-finger Oxford Heliox ^3He system combined with a ^4He Oxford Variox cryostat was used to reach temperatures down to 250 mK. By employing active compensation coils, true zero-field (ZF) conditions could be achieved during the ZF- μSR experiments.

C. *Ab initio* calculations

We performed nonspinpolarized band structure calculations for $\text{Ce}_3\text{Bi}_4\text{Pd}_4$ based on density functional theory, treating the Ce $4f$ electrons in the open-core approximation and taking spin-orbit interaction into account. Weyl nodes in the k_x - k_z plane of the Brillouin zone were identified via their Berry curvature (see the Supplementary Information for further details).

D. Model calculations

We extended the model for a Weyl-Kondo semimetal¹¹ to include beyond nearest-neighbor hopping terms, and solved the self-consistent saddle-point equations for the strong interaction limit

of the periodic Anderson model. We find a Weyl-Kondo solution with tilted Weyl cones. With the Kondo interaction placing the Fermi energy very close to the Weyl nodes, the Fermi surface comprises Fermi pockets that are asymmetrically distributed near the Weyl and anti-Weyl nodes. The Berry curvature, which diverges exactly at any Weyl or anti-Weyl node, is thus very large on the Fermi surface (see the Supplementary Information for further details).